Nanoscale

PAPER

View Article Online
View Journal | View Issue

Cite this: *Nanoscale*, 2025, **17**, 2215

Comprehensive determination of highly symmetric transition metal dichalcogenide multilayers†

Jessica Arcudia,*[a,b] Filiberto Ortíz-Chi,[c] Jorge Barroso[d] and Gabriel Merino*[a]

Received 9th September 2024,
Accepted 22nd November 2024

DOI: 10.1039/d4nr03696d

rsc.li/nanoscale

This study expands the JAM notation to systematically explore stacking configurations of transition metal dichalcogenide (TMDC) multilayers, covering both conventional and Janus structures. We extended JAM to represent four TMDC types: 1H, 1T, Janus 1H, and Janus 1T, adding characters to describe these structures. Additionally, we updated the JAM algorithm to generate stacking configurations and produce VASP-compatible POSCAR files. Using bilayer MoSSe as a model system, we analyzed stability, band gap, and interlayer interactions across all stackings. This expanded JAM approach enables detailed exploration of TMDC multilayers and supports further research into 2D materials.

Introduction

Transition metal dichalcogenides (TMDCs) are 2D materials with a honeycomb lattice structure, consisting of a transition metal layer sandwiched between two layers of chalcogen atoms,[1] with MoS_2 as the example *par excellence*. The unit cell of monolayer MoS_2 can adopt two configurations: 1H and 1T. The key difference lies in the occupancy of highly symmetric sites within the unit cell, labeled **1*a***, **1*b***, and **1*c***. In the 1H phase, only two sites are occupied, while in the 1T phase, all three are filled (see Fig. 1). The structural variations significantly affect the material's properties, particularly its electronic behavior. For example, the 1H-MoS_2 phase is a semiconductor with a direct band gap,[2] while the 1T-MoS_2 phase is metallic and typically metastable.[3] However, stability in the 1T phase can be achieved through Re atom doping or Li atom adsorption.[4,5]

Janus TMDCs are a distinct type of 2D TMDCs characterized by an asymmetrical arrangement within their unit cell. Unlike conventional TMDCs, Janus TMDCs have different chalcogen atoms on opposite sides of the lattice (*e.g.*, sulfur on one side and selenium on the other),[6,7] which gives rise to single properties, such as an intrinsic vertical dipole absent in standard 2D TMDCs. Fig. 1c and d shows the unit cell of a Janus TMDC in both the 1H and 1T phases.

An example of a Janus TMDC is the MoSSe monolayer, which has attracted attention due to its exceptional properties and potential applications,[8,9] including electronic, optical,[10] and mechanical properties,[11] as well as its suitability for applications such as water splitting,[12] Li-ion batteries,[13] and gas sensing.[14] These attributes position Janus MoSSe as a promising candidate for optoelectronic and valleytronic devices.[15]

Studies on bilayer MoSSe have shown its advantages over the monolayer, particularly in photocatalytic water splitting, enhancing its potential for solar energy conversion.[16] Theoretical studies suggest that bilayer MoSSe effectively suppresses carrier recombination, crucial for optoelectronic devices.[17] Additionally, its shows promise as an anode material in lithium-ion batteries, highlighting its importance in energy storage technologies.[18] Despite extensive research on bilayer stacking configurations, a standardized nomenclature is still lacking.

We developed a linear character string system, the Joining and Arrangement of Multilayers (JAM) notation, to represent four specific types of layered materials: planar (PL), binary planar (BPL), buckled (BU), and binary buckled (BBU), as depicted in Fig. 2. Using geometrical data, JAM can reconstruct a honeycomb lattice of layers and determine their stacking sequences.[19] This approach has been useful in determining all possible layer arrangements, as shown in our recent studies of phosphorene and AsP bilayers.[20,21] However, a key question arises: Can JAM's capabilities be extended to TMDC materials? For example, MoS_2 shares a similar lattice structure with the materials in Fig. 2 but differs in that its monolayer unit cell contains three atoms instead of two.

To address this, we expanded the JAM notation system to include four TMDC variants: 1H, 1T, Janus 1H, and Janus 1T. This expansion introduces new characters to represent the

[a]*Departamento de Física Aplicada, Centro de Investigación y de Estudios Avanzados, Unidad Mérida, km 6 Antigua carretera a Progreso, Apdo. Postal 73, Cordemex 97310, Mérida, Yuc., Mexico. E-mail: jessica.arcudia@cinvestav.mx, gmerino@cinvestav.mx*
[b]*Department of Physics, University of Texas, Dallas, 800 W. Campbell Rd, Richardson, Texas 75080, USA*
[c]*Conahcyt-Departamento de Física Aplicada, Centro de Investigación y de Estudios Avanzados, Unidad Mérida, Mérida, Yucatán, México*
[d]*Department of Chemistry, Clemson University, Clemson, South Carolina 29634, USA*

† Electronic supplementary information (ESI) available. See DOI: https://doi.org/10.1039/d4nr03696d

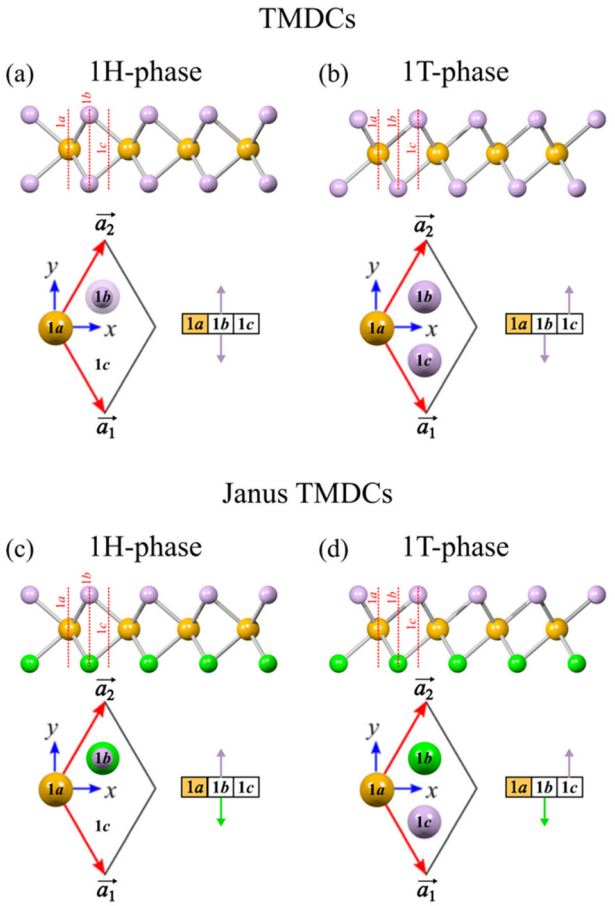

Fig. 1 Lateral views, unit cells, and block diagrams of TMDCs and Janus TMDCs. (a)–(b) TMDCs in the 1H and 1T phases; (c)–(d) Janus TMDCs in the 1H and 1T phases.

composition and structure of both TMDCs and Janus TMDCs. Using MoSSe as a case study, we employed JAM to identify all possible bilayer stacking arrangements, which were characterized in terms of energetic stability and electronic properties, such as bandgap. This approach lays the foundation for exploring a broader range of 2D materials, highlighting the importance of controlled layer stacking in advancing materials science and electronics.

Computational details

Density Functional Theory (DFT) computations were performed using the projector-augmented wave (PAW) method,[22,23] as implemented in VASP.[24,25] Ion-electron interactions were described using PAW potentials from the VASP library, with valence states expanded into plane waves with a 550 eV energy cutoff. Geometry optimizations were carried out with the *meta*-GGA SCAN-rVV10 functional.[26] For Brillouin zone sampling, a Γ-centered *k*-grid of 15 × 15 × 1 *k*-points with 0.10 eV Gaussian smearing was used. Convergence criteria were set to 10^{-8} eV for the total energy and 10^{-3} eV Å^{-1} for atomic forces.

Each bilayer was represented by its minimum unit cell, with each MoSSe layer consisting of three atoms in Wyckoff positions, requiring only six atoms to define the bilayer unit cell. This setup ensures periodicity in the *XY*-plane, with periodic boundary conditions along the *Z*-axis falling into two categories:[27] the first involves boundary conditions invariant under $Z \rightarrow -Z$ symmetry (*e.g.*, AA-type bilayers), and the second involves asymmetric boundary conditions (*e.g.*, AB-type bilayers). A wide vacuum space (18 Å) along *Z* was used to prevent significative interactions between periodic images.

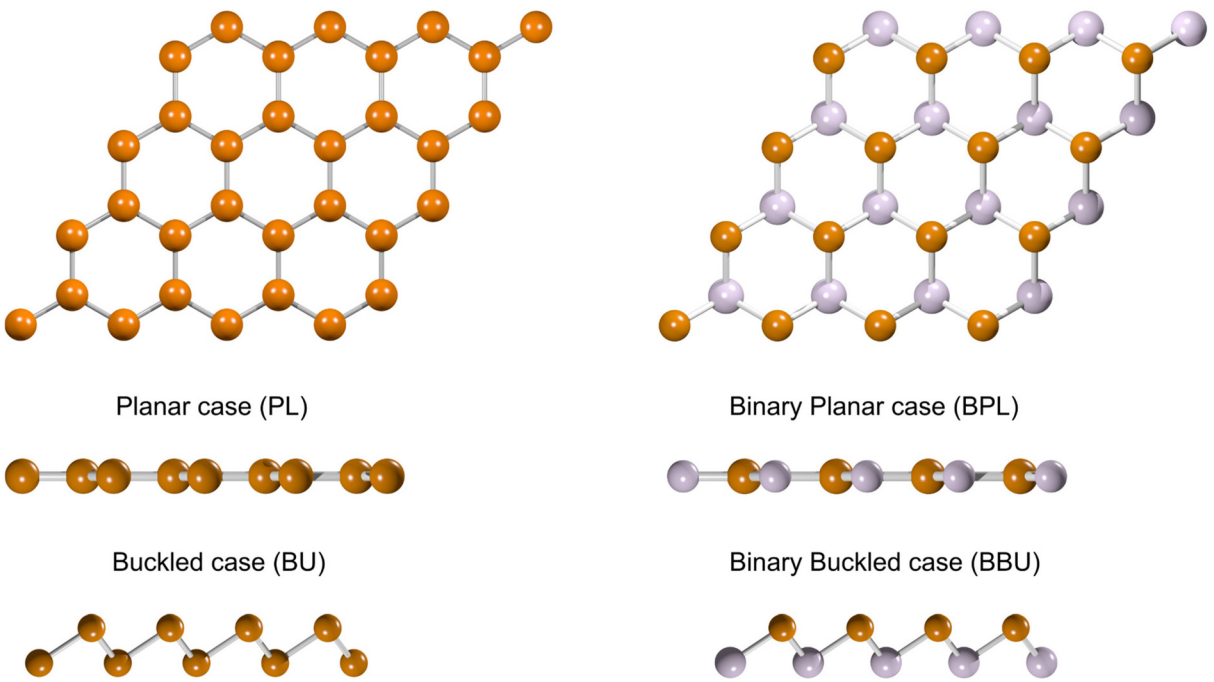

Fig. 2 The four types of layered-structured materials represented by JAM notation.

Electronic structures were calculated using the PBE functional[28] with spin–orbit coupling, while phonon calculations were carried out using the small displacement method with 5 × 5 × 1 supercells *via* the Phonopy code.[29] Note that this study does not aim to determine the global minimum structure of each stacking configuration, as such an analysis would require an extensive search across various crystalline phases and dimensionalities. Moreover, the experimental validity of multilayers is well-established.[30,31]

To analyze interlayer interactions, Periodic Energy Decomposition Analysis (PEDA)[32–34] was performed using the *meta*-GGA SCAN-D3 functional with a Slater-type TZP basis set and Grimme's D3 approximation for dispersion. PEDA decomposes the interaction energy (ΔE_{int}) into electrostatic ($\Delta V_{\mathrm{elstat}}$), orbital ($\Delta E_{\mathrm{orb}}$), dispersion ($\Delta E_{\mathrm{disp}}$), and Pauli repulsion ($\Delta E_{\mathrm{Pauli}}$) components:

$$\Delta E_{\mathrm{int}} = \Delta E_{\mathrm{Pauli}} + \Delta V_{\mathrm{elstat}} + \Delta E_{\mathrm{orb}} + \Delta E_{\mathrm{disp}}$$

The electrostatic interaction is typically attractive and represents the energy between the unperturbed charge distributions of the prepared fragments. Pauli repulsion accounts for steric repulsion, consisting of destabilizing interactions between occupied orbitals of the fragments. Orbital interactions involve charge transfer and polarization effects, while the dispersion term captures van der Waals forces from medium- and long-range interactions. These calculations were performed using the BAND package.[52]

JAM construction

Let us begin with the 1H phase of TMDC materials, where two lattice sites are occupied: one by two chalcogen atoms and the other by the transition metal, or "central atom" (depicted in orange in Fig. 1). Since the central atom lies on the basal plane, it is represented as a colored box rather than an arrow.

In JAM notation, the central atom is denoted by an asterisk, and the chalcogen atoms are enclosed in parenthesis to indicate shared site occupancy. Fig. 3a shows a TMDC bilayer in the 1H phase. The central atom eclipses the chalcogen pair at site **1*a*** (**j*, (+*k* − *k*)), while at site **1*b***, the chalcogen pair in the upper layer eclipses the central atom in the lower layer ((+*k* − *k*), **j*), with site **1*c*** remaining vacant. Thus, the JAM for this arrangement is **j* (+*k* − *k*)/(+*k* − *k*)**j*/00.

Fig. 3c depicts a Janus TMDC bilayer (such as MoSSe) in the 1H phase. In this case, eclipsed atoms occupy only site **1*b***, where the upper chalcogen pair interacts with the lower central atom ((+*k* − *l*),**j*). At site **1*a***, only the upper central atom is present (**j*, 0), and at site **1*c***, only the lower chalcogen pair is positioned (0, (+*k* − *l*)). The corresponding JAM is **j*0/(*k* − *l*)**j*/0(*k* − *l*).

Next, consider the 1T phase, where all three high-symmetry sites are occupied, eliminating the need for "0" in the JAM notation. In other words, every site contains eclipsed atoms. Fig. 3b shows a TMDC bilayer in the 1T phase, where the eclipsed atoms from top to bottom include a central atom with the *k*-type atom at site **1*a***, downward and upward-oriented chalcogen atoms (−*k*, *k*) at site **1*b***, and an upward *k*-type atom with a central atom (+*k*, **j*) at site **1*c***. The JAM for this arrangement is **j* − *k*/−*kk*/*k*j*.

For a Janus TMDC bilayer (Fig. 3d), the eclipsed atoms include central atoms at site **1*a***, downward *l*-type atoms at site **1*b***, and upward *k*-type atoms at site **1*c***. The resulting JAM is **j*j*/−*l* − *l*/*kk*.

To identify equivalent JAM sequences, we use rules similar to those for PL, BPL, BU, and BBU materials.[19] This involves applying translational and reflection symmetries within the JAM algorithm to derive canonical JAMs, with the specific sequence depending on the canonicalization algorithm used. Translational symmetry in the honeycomb lattice, due to its periodicity, allows cyclic permutations at the lattice sites (**1*a***, **1*b***, and **1*c***). Thus, if the three columns of a multilayer array (as depicted in Fig. 3) appear in the same order as those in another system's array, the stacking configurations are equivalent, regardless of order. Reflection symmetry means that when the multilayer system is mirrored across the horizontal plane, the layer order reverses. When comparing two JAMs in a matrix array (Fig. 3), the rows are flipped top-to-bottom and inverted. If the JAMs remain identical after this operation, the stacking sequences are equivalent. For detailed mathematical treatment, please refer to the original publication on JAM.[19]

Sign changes are irrelevant to the central atom in TMDCs and Janus TMDCs, as it lacks out-of-plane displacement. Additionally, in 1H-phase systems (where two atoms share a lattice site), the sign change associated with reflection affects both characters within the parentheses; for example, (+*k* − *l*) changes to (*k* + *l*). Table 1 lists the non-equivalent stacking sequences for these materials. For MoS_2 bilayers, five canonical JAMs emerge from 36 possible combinations in both the 1H and 1T phases; for trilayers, 21; tetralayers, 120; and pentalayers, 666. In contrast, Janus MoSSe has many more: 16 for bilayers, 144 for trilayers, 1776 for tetralayers, and 20 736 for pentalayers in both phases. This expanded JAM notation supports a broader range of 2D materials, offering a comprehensive structural representation. The updated JAM algorithm, inclusive of TMDCs and Janus TMDCs, is available on our GitHub page.[35]

Janus MoSSe bilayers

Fig. 4 displays the sixteen possible stacking arrangements for bilayer 1H-MoSSe, along with their JAMs and relative SCAN-rVV10 energies (ΔE). We categorized these configurations based on three criteria: energetic stability, AB-type notation, and JAM strings. The AB-type notation, adapted from hexagonal boron nitride studies,[36] identifies five stacking types: AA′ (eclipsed Mo over SSe), AB (staggered Mo over SSe), A′B (staggered Mo over Mo), AA (eclipsed with Mo over Mo and SSe over SSe), and AB′ (staggered with SSe over SSe).

All configurations share lattice constants of 3.23 Å and out-of-plane buckling of 3.22 Å. The Mo–S and Mo–Se bond

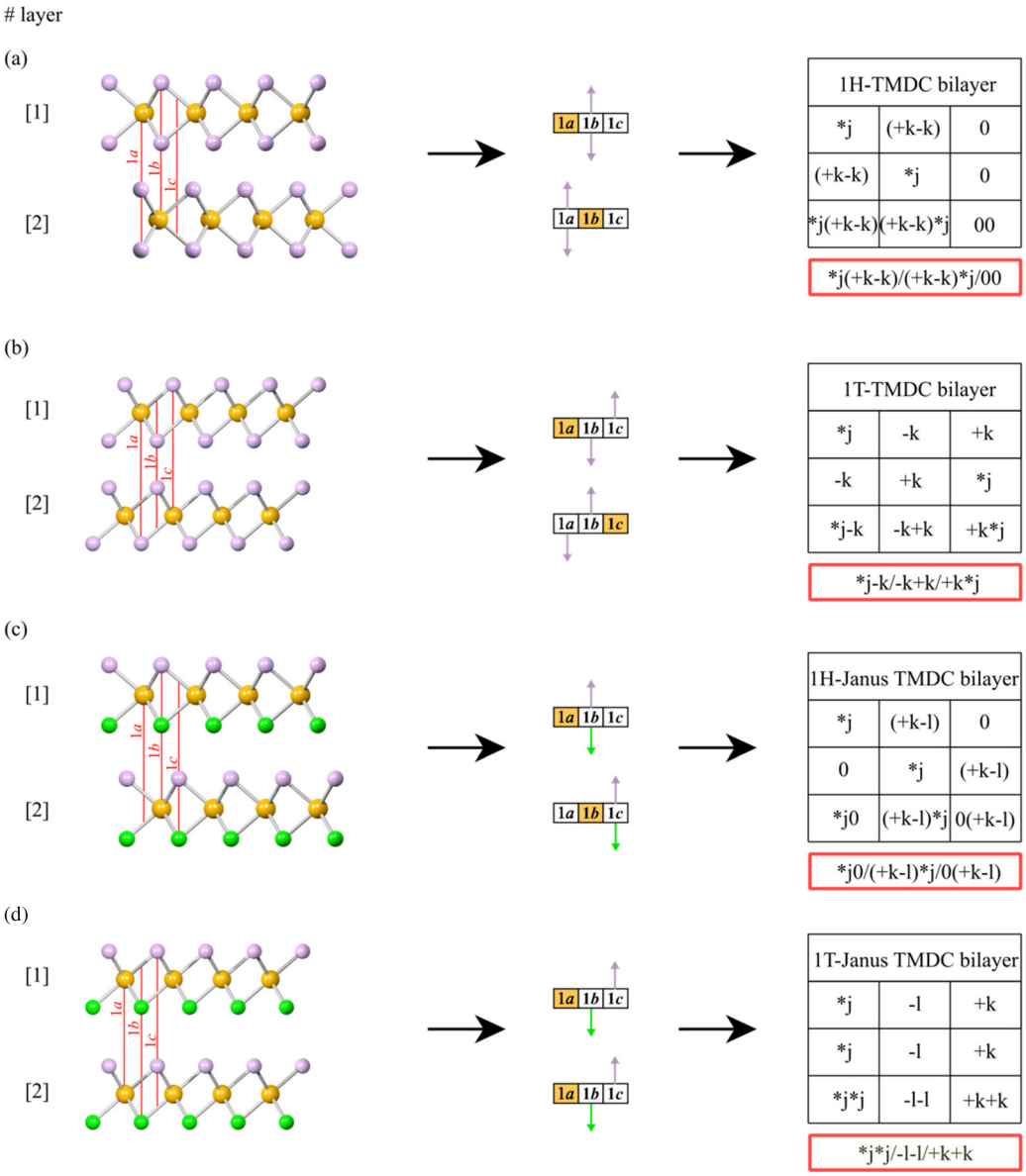

Fig. 3 JAM notation for a (a) 1H-TMDC, (b) 1T-TMDC, (c) 1H-Janus TMDC, and (d) 1T-Janus TMDC bilayers.

Table 1 Stacking sequences of a TMDC and Janus TMDC material using JAM notation. The total number of possibilities, generated by considering all the combinations, is shown in parentheses

	Number of layers			
Type of material	**2**	**3**	**4**	**5**
1H-TMDC	5 (36)	21 (216)	120 (1296)	666 (7776)
1T-TMDC	5 (36)	21 (216)	120 (1296)	666 (7776)
1H-Janus TMDC	16 (144)	144 (1728)	1776 (20 736)	20 736 (248 832)
1T-Janus TMDC	16 (144)	144 (1728)	1776 (20 736)	20 736 (248 832)

lengths are 2.41 and 2.52 Å, respectively, consistent with those in the monolayer.[37–39] The two lowest-energy polytypes, differing by just 0.13 meV per atom, have JAM sequences *Mo(+S–Se)/(+S–Se)*Mo/00 and Mo(S–Se)/(S–Se)0/0Mo with S–Se interlayer distances of 3.17 and 3.20 Å, respectively (Table 2). The third polytype, 0.39 meV per atom higher, has the JAM sequence *Mo(–S + Se)/(S–Se)*Mo/00, with Se–Se distances longer than 3.31 Å. In these three polytypes, at least one Mo atom aligns with a chalcogen, as indicated by the "*Mo–(S–Se)" pairing in the JAM sequence (Fig. 4). This alignment indicates lateral chalcogen–chalcogen interactions between the layers, leading to closer interlayer distances.

These three systems have been widely studied,[12,13,16,37,38,40–46] particularly the first two, and our reported interlayer distances align with previous findings.

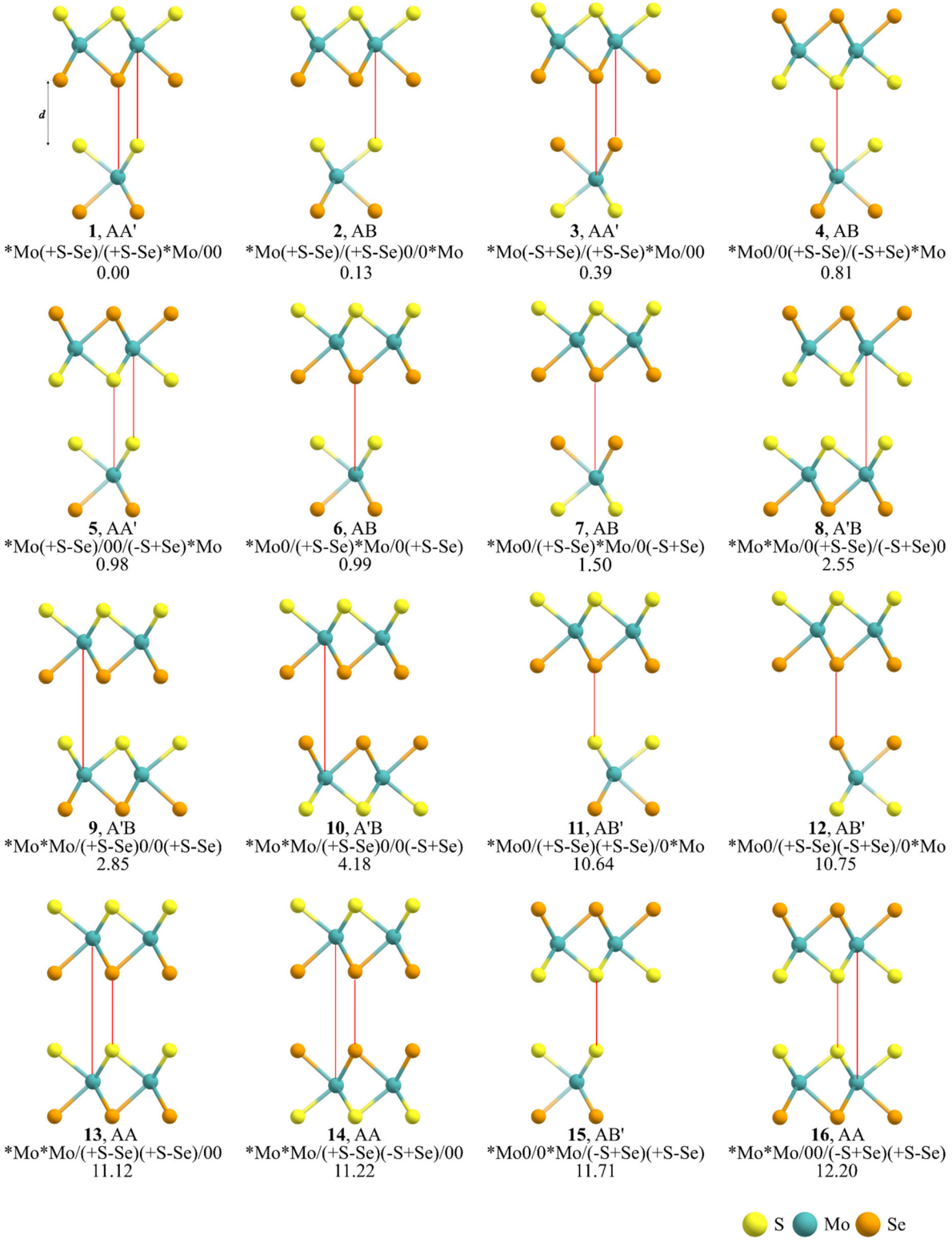

Fig. 4 JAM strings of the sixteen stacking configurations of bilayer MoSSe. Relative energies (ΔE) in meV per atom computed at the SCAN-rVV10 level. Red lines indicate eclipsed atoms.

Based on theoretical approaches, interlayer distances for the first, second, and third bilayers typically fall within 3.1–3.15 Å, 2.91–3.21 Å, and 3.20–3.22 Å, respectively. Few studies, however, have compared the energies of all three stacking sequences. Some indicate the third polytype as the most stable, with an energy difference under 10 meV per atom when

Table 2 Interlayer distances (d) in Å, dipole moments (μ) in Debye, band gap (E_g) with spin–orbit coupling in eV, and results of PEDA in kcal mol^{-1}, considering as interacting fragments each layer of the sixteen stacking configurations of bilayer MoSSe. The values between parentheses show the percentage of the attractive contributions

	d	μ	E_g	ΔE_{int}	ΔE_{Pauli}	ΔE_{orb}	ΔV_{elstat}	ΔE_{disp}
1	3.20	0.33	0.90	−5.35	3.43	−2.70 (30.8)	−2.70 (30.8)	−3.38 (38.5)
2	3.17	0.32	0.92	−5.40	3.82	−2.91 (31.6)	−2.89 (31.4)	−3.41 (37.0)
3	3.31	0.00	1.32	−5.37	3.62	−2.67 (29.7)	−2.98 (33.2)	−3.33 (37.1)
4	3.05	0.02	0.97	−5.35	3.73	−2.89 (31.9)	−2.71 (29.9)	−3.47 (38.3)
5	3.10	0.00	1.04	−5.23	3.06	−2.55 (30.8)	−2.34 (28.2)	−3.40 (41.0)
6	3.21	0.34	0.87	−5.23	3.43	−2.64 (30.4)	−2.68 (30.9)	−3.36 (38.7)
7	3.32	0.01	1.34	−5.26	3.65	−2.63 (29.5)	−2.97 (33.3)	−3.32 (37.2)
8	3.11	0.00	1.02	−5.02	3.13	−2.49 (30.6)	−2.27 (27.9)	−3.39 (41.6)
9	3.25	0.33	0.92	−4.95	3.15	−2.38 (29.4)	−2.40 (29.7)	−3.31 (40.9)
10	3.44	0.00	1.41	−4.80	2.52	−1.97 (26.9)	−2.19 (29.9)	−3.16 (43.2)
11	3.74	0.34	0.95	−3.46	1.05	−1.04 (23.1)	−0.79 (17.5)	−2.68 (59.4)
12	3.82	0.00	1.50	−3.59	1.37	−1.05 (21.2)	−1.21 (24.4)	−2.69 (54.3)
13	3.75	0.34	0.96	−3.40	1.22	−0.99 (21.4)	−0.96 (20.8)	−2.67 (57.8)
14	3.85	0.00	1.45	−3.51	1.22	−0.96 (20.3)	−1.11 (23.5)	−2.66 (56.2)
15	3.65	0.00	1.27	−3.34	1.18	−1.02 (22.6)	−0.83 (18.4)	−2.67 (59.1)
16	3.66	0.00	1.27	−3.28	1.16	−0.97 (21.8)	−0.81 (18.2)	−2.66 (59.9)

using Grimme's DFT-D2 correction.[12,13,16,17,31,32,35–38] Wei *et al.* applied several methods, including Grimme's D3-Zero Damping, D3-Becke–Johnson Damping, and the Tkatchenko–Scheffler method, finding that energy rankings vary by methods[16] due to the minor differences between polytypes. Phonon calculations confirm the stability of the top three polytypes, with no imaginary frequencies obtained (Fig. S1†).

Polytypes **4** through **7**, with relative energies from 0.81 to 1.50 meV per atom, are energetically close to the top three and share AA′ and AB stacking types, each with at least one Mo atom aligned with a chalcogen, as shown by the "*Mo(S–Se)" characters in their JAMs. In contrast, polytypes **8** through **10**, with energies between 2.55 and 4.18 meV per atom, exhibit A′B stacking, where Mo atoms in both layers are eclipsed, resulting in the appearance of the "*Mo*Mo" characters in their JAM sequences. The differences among these polytypes are the type of interlayer interactions (S–S, S–Se, or Se–Se). Interestingly, while the ten most stable configurations correspond to AA′, AB, and A′B stacking, the six highest-energy configurations (over 10 meV per atom) have longer interlayer distances of 3.66–3.85 Å (Table 2) and involve direct chalcogen overlap. Their JAM sequences include characters like "(Se–Se)(S–Se)" with varying signs. It is worth noting that sequences **8**, **10**, and **12** for Janus MoSSe bilayers, with JAM sequences *Mo*Mo/0(S–Se)/(–SSe)0, *Mo*Mo/(S–Se)0/0(–S + Se), and *Mo0/(S–Se)(–S + Se)/0Mo, have not been reported.

Although SCAN-rVV10 calculations were chosen for their reliability with layered materials,[47] we recognize that energy and interlayer distances may vary by theoretical approach. To evaluate this, we optimized all 16 stacking configurations using PBE+D3[48] and optB86b-vdW[49] (Table S1†), finding consistent results in energy stability and interlayer distances. The three most stable configurations were consistent across methods, with energy differences within 1 meV per atom, and the six highest-energy configurations remained unchanged.

We examined the electronic properties of different stacking sequences, finding all systems to be semiconductors with band gaps between 0.90 and 1.50 eV (Table 2), lower than the direct band gap of 1.52 eV found in the monolayer (Fig. S2†). Unlike the monolayer, the two lowest-energy configurations have indirect band gaps, with the smallest values at 0.90 and 0.92 eV (Fig. 5). For polytype 2, the indirect band gap is consistent with the findings of Zhong *et al.*,[13] although Wei *et al.* report it as direct.[16]

Only polytypes **11** and **13**, with eclipsed S–Se pairs in interlayer interactions, retain a direct band gap similar to that of the monolayer, with both the conduction band minimum (CBM) and valence band maximum (VBM) at the K point. In contrast, the other configurations show indirect band gaps, with the VBM shifting to the Γ point (Fig. S3†), consistent with previous studies.[12,13,16,17,37,38,40–42,44] The key distinction for polytypes **11** and **13** is their face-to-face S–Se interlayer distances, unlike those in polytype **1**, where the S–Se interactions are lateral.

Interestingly, stacking arrangements with S–Se interactions and dipole moments correlate with lower bandgaps, ranging from 0.87 to 0.96 eV. The two most stable configurations, with dipole moments of 0.33 and 0.32 D, also have low bandgaps of 0.90 and 0.92 eV. Configurations with S–S interactions follow, with bandgaps from 0.97 to 1.27 eV, while those with Se–Se interactions have the highest bandgaps, from 1.32 to 1.50 eV. Electron density maps show minimal variation among the 16 bilayers (Fig. S4†), suggesting that interlayer interactions are mainly due to long-range dispersion forces.

To further explore the interlayer interactions, we performed a periodic energy decomposition analysis (PEDA).[34] Although the interaction energies (ΔE_{int}) from SCAN-D3/TZP vary modestly (−5.40 to −3.28 kcal mol^{-1}), their ranking is consistent with that in SCAN-rVV10 predictions. An inverse relationship is found between the orbital contributions and Pauli repulsion: lower-energy configurations, with shorter interlayer distances, show higher orbital contributions (exceeding 29%, or −2.91 and −2.38 kcal mol^{-1}) in sequences **1–9**. In contrast, higher energy polytypes (with interlayer distances over 3.6 Å)

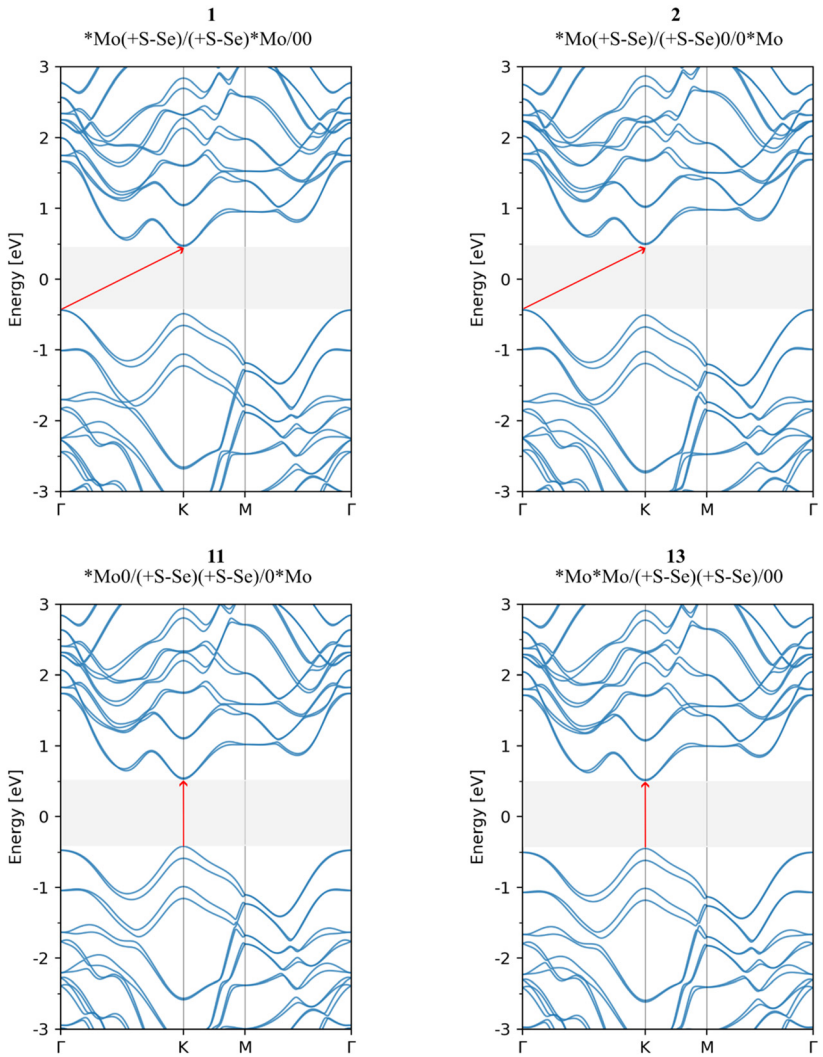

Fig. 5 Electronic band structure of **1**, **2**, **11**, and **13** stacking sequences of bilayer MoSSe.

have lower orbital contributions, from −1.97 to −0.96 kcal mol^{-1}. As layers approach, Pauli repulsion increases.

On the other hand, the dispersion energy (ΔE_{disp}) is the main attractive force, contributing 37.0 to 59.9% of the total interaction energy (Table 2). Our analysis indicates that electrostatic and dispersion energies counterbalance each other. In higher-energy polytypes (**11–16**), ΔE_{disp} constitutes 54.3 to 59.9% of the interaction energy, reducing the electrostatic component to 17.5–24.4%. In contrast, in lower-energy polytypes (**1–7**), ΔE_{disp} contributes 37.0 to 41.0%, while the electrostatic term ranges from 28.2 to 33.2%. This pattern highlights the increasing role of van der Waals forces and the importance of medium- and long-range interactions in bilayers.

Conclusions

We extended the JAM notation—a linear string-based system—to cover four types of transition metal dichalcogenides (TMDCs): 1H, 1T, Janus 1H, and Janus 1T. This extension facilitates the reconstruction of honeycomb lattice structures and represents various stacking sequences, including those in materials with three-atom unit cells, like MoS_2.

Using this expanded JAM notation, we identified and characterized all possible stacking arrangements for MoSSe bilayers, a Janus TMDC. Sixteen distinct stacking configurations were evaluated for energetic stability and electronic properties, including bandgap variations. Three configurations showed competitive stability: *Mo(S–Se)/(S–Se)*Mo/00, Mo(S–Se)/(S–Se)0/0Mo, and *Mo(–S + Se)/(S–Se)*Mo/00, each with interlayer distances under 3.30 Å and indirect band gaps of 0.90, 0.92, and 1.32 eV, respectively, in contrast to the monolayer's direct gap of 1.52 eV. Our findings highlight how interlayer interactions and symmetry significantly impact the electronic nature of MoSSe bilayers, with S–Se interactions at eclipsed positions notably affecting band gap values and type.

PEDA calculations show that the lowest-energy, closest-spaced configurations have the highest orbital contributions,

with dispersion energy as the dominant attractive force (37.0%–59.9% of the total interaction energy). Thus, interlayer distance is crucial for determining the stability and electronic properties, underscoring the importance of van der Waals forces and long-range interactions in 2D bilayer studies.

The expanded JAM notation is a robust tool for examining stacking sequences and advancing TMDC multilayer research. Mastering the stacking arrangements is essential for applications in optoelectronics. This work lays the foundation for future studies on diverse 2D materials, facilitating the design of novel materials with customized properties. Furthermore, the multilayer structures derived from JAM can be effectively analyzed *via* machine learning interatomic potentials, trained on smaller cases to predict properties for larger configurations, as demonstrated for the 2D material family.[50,51]

Data availability

The data supporting this article have been included as part of the ESI.†

Conflicts of interest

There are no conflicts to declare.

Acknowledgements

This work was funded by Conahcyt (Grant Conacyt Ciencia Básica y/o Ciencia de Frontera No. 320362, Proyecto Sinergia 1561802, and Grant #A1-S-45886). J. A. thanks Conahcyt for support through her Postdoc fellowship. Computations supporting this project were performed on High-Performance Computing systems at Cinvestav (Xiuhcoatl) and the Palmetto Cluster at Clemson University. This material is based on work supported by the National Science Foundation under Grant Nos. MRI# 2024205, MRI# 1725573, and CRI# 2010270.

References

1 M. Chhowalla, H. S. Shin, G. Eda, L.-J. Li, K. P. Loh and H. Zhang, *Nat. Chem.*, 2013, **5**, 263–275.
2 E. S. Kadantsev and P. Hawrylak, *Solid State Commun.*, 2012, **152**, 909–913.
3 M. Calandra, *Phys. Rev. B: Condens. Matter Mater. Phys.*, 2013, **88**, 245428.
4 A. N. Enyashin, L. Yadgarov, L. Houben, I. Popov, M. Weidenbach, R. Tenne, M. Bar-Sadan and G. Seifert, *J. Phys. Chem. C*, 2011, **115**, 24586–24591.
5 H. Wang, Z. Lu, S. Xu, D. Kong, J. J. Cha, G. Zheng, P.-C. Hsu, K. Yan, D. Bradshaw, F. B. Prinz and Y. Cui, *Proc. Natl. Acad. Sci. U. S. A.*, 2013, **110**, 19701–19706.
6 L. Dong, J. Lou and V. B. Shenoy, *ACS Nano*, 2017, **11**, 8242–8248.
7 Y. Guo, S. Zhou, Y. Bai and J. Zhao, *Appl. Phys. Lett.*, 2017, **110**, 163102.
8 A.-Y. Lu, H. Zhu, J. Xiao, C.-P. Chuu, Y. Han, M.-H. Chiu, C.-C. Cheng, C.-W. Yang, K.-H. Wei, Y. Yang, Y. Wang, D. Sokaras, D. Nordlund, P. Yang, D. A. Muller, M.-Y. Chou, X. Zhang and L.-J. Li, *Nat. Nanotechnol.*, 2017, **12**, 744–749.
9 J. Zhang, S. Jia, I. Kholmanov, L. Dong, D. Er, W. Chen, H. Guo, Z. Jin, V. B. Shenoy, L. Shi and J. Lou, *ACS Nano*, 2017, **11**, 8192–8198.
10 R. Li, Y. Cheng and W. Huang, *Small*, 2018, **14**, e1802091.
11 M. Meng, T. Li, S. Li and K. Liu, *J. Phys. D: Appl. Phys.*, 2018, **51**, 105004.
12 Z. Guan, S. Ni and S. Hu, *J. Phys. Chem. C*, 2018, **122**, 6209–6216.
13 L. Zhong, X. Li, Y. Pu, M. Wang, C. Zhan and X. Xiao, *Phys. Chem. Chem. Phys.*, 2024, **26**, 1030–1038.
14 Q. Wu, L. Cao, Y. S. Ang and L. K. Ang, *Nano Express*, 2020, **1**, 010042.
15 B. Hou, Y. Zhang, H. Zhang, H. Shao, C. Ma, X. Zhang, Y. Chen, K. Xu, G. Ni and H. Zhu, *J. Phys. Chem. Lett.*, 2020, **11**, 3116–3128.
16 S. Wei, J. Li, X. Liao, H. Jin and Y. Wei, *J. Phys. Chem. C*, 2019, **123**, 22570–22577.
17 B. Song, L. Liu and C. Yam, *J. Phys. Chem. Lett.*, 2019, **10**, 5564–5570.
18 C. Shang, X. Lei, B. Hou, M. Wu, B. Xu, G. Liu and C. Ouyang, *J. Phys. Chem. C*, 2018, **122**, 23899–23909.
19 J. Arcudia, F. Ortíz-Chi, A. Sánchez-Valenzuela, A. Aspuru-Guzik and G. Merino, *Matter*, 2023, **6**, 1503–1513.
20 J. Arcudia, R. Kempt, M. E. Cifuentes-Quintal, T. Heine and G. Merino, *Phys. Rev. Lett.*, 2020, **125**, 196401.
21 J. Arcudia, B. Emrem, T. Heine and G. Merino, *Nanoscale*, 2022, **14**, 10136.
22 P. E. Blöchl, *Phys. Rev. B: Condens. Matter Mater. Phys.*, 1994, **50**, 17953–17979.
23 G. Kresse and D. Joubert, *Phys. Rev. B: Condens. Matter Mater. Phys.*, 1999, **59**, 1758–1775.
24 G. Kresse and J. Furthmüller, *Comput. Mater. Sci.*, 1996, **6**, 15–50.
25 G. Kresse and J. Furthmüller, *Phys. Rev. B: Condens. Matter Mater. Phys.*, 1996, **54**, 11169–11186.
26 H. Peng, Z.-H. Yang, J. P. Perdew and J. Sun, *Phys. Rev. X*, 2016, **6**, 041005.
27 M. Mazars, *Phys. Rep.*, 2011, **500**, 43–116.
28 J. P. Perdew, K. Burke and M. Ernzerhof, *Phys. Rev. Lett.*, 1996, **77**, 3865–3868.
29 A. Togo and I. Tanaka, *Scr. Mater.*, 2015, **108**, 1–5.
30 H. Li, J. Wu, Z. Yin and H. Zhang, *Acc. Chem. Res.*, 2014, **47**, 1067–1075.
31 X. Zhang, X.-F. Qiao, W. Shi, J.-B. Wu, D.-S. Jiang and P.-H. Tan, *Chem. Soc. Rev.*, 2015, **44**, 2757–2785.
32 G. te Velde, F. M. Bickelhaupt, E. J. Baerends, C. Fonseca Guerra, S. J. A. van Gisbergen, J. G. Snijders and T. Ziegler, *J. Comput. Chem.*, 2001, **22**, 931–967.
33 G. te Velde and E. J. Baerends, *Phys. Rev. B: Condens. Matter Mater. Phys.*, 1991, **44**, 7888–7903.

34 M. Raupach and R. Tonner, *J. Chem. Phys.*, 2015, **142**, 194105.
35 **https://github.com/Theochem-merida/xjam.git**. (Accessed August 29, 2024).
36 G. Constantinescu, A. Kuc and T. Heine, *Phys. Rev. Lett.*, 2013, **111**, 036104.
37 C. Shang, B. Xu, X. Lei, S. Yu, D. Chen, M. Wu, B. Sun, G. Liu and C. Ouyang, *Phys. Chem. Chem. Phys.*, 2018, **20**, 20919–20926.
38 W.-J. Yin, B. Wen, G.-Z. Nie, X.-L. Wei and L.-M. Liu, *J. Mater. Chem.*, 2018, **6**, 1693–1700.
39 Y. Ji, M. Yang, H. Lin, T. Hou, L. Wang, Y. Li and S.-T. Lee, *J. Phys. Chem. C*, 2018, **122**, 3123–3129.
40 Y. Yang, Y. Zhang, H. Ye, Z. Yu, Y. Liu, B. Su and W. Xu, *Superlattices Microstruct.*, 2019, **131**, 8–14.
41 F. Li, W. Wei, H. Wang, B. Huang, Y. Dai and T. Jacob, *J. Phys. Chem. Lett.*, 2019, **10**, 559–565.
42 C. Long, Y. Dai, Z.-R. Gong and H. Jin, *Phys. Rev. B*, 2019, **99**, 115316.
43 G. Chaney, A. Ibrahim, F. Ersan, D. Çakır and C. Ataca, *ACS Appl. Mater. Interfaces*, 2021, **13**, 36388–36406.
44 X. Zhang, R. Pang, X. Hou and S. Wang, *New J. Phys.*, 2021, **23**, 013003.
45 Z. Jia, H. Zhang, X. Chen and W. Ding, *J. Electron. Mater.*, 2023, **52**, 2458–2465.
46 L. Lin, X. Hu, R. Meng, X. Li, Y. Guo, H. Da, Y. Jiang, D. Wang, Y. Yang and X. Yan, *Nanoscale*, 2024, **16**, 4841–4850.
47 B. Emrem, R. Kempt, K. Finzel and T. Heine, *Adv. Theory Simul.*, 2022, **5**, 2200055.
48 S. Grimme, J. Antony, S. Ehrlich and H. Krieg, *J. Chem. Phys.*, 2010, **132**, 154104.
49 J. Klimeš, D. R. Bowler and A. Michaelides, *Phys. Rev. B: Condens. Matter Mater. Phys.*, 2011, **83**, 195131.
50 I. S. Novikov, K. Gubaev, E. V. Podryabinkin and A. V. Shapeev, *Mach. Learn. Sci. Technol.*, 2021, **2**, 025002.
51 B. Mortazavi, B. Javvaji, F. Shojaei, T. Rabczuk, A. V. Shapeev and X. Zhuang, *Nano Energy*, 2021, **82**, 105716.
52 P. H. T. Philipsen, G. te Velde, E. J. Baerends, J. A. Berger, P. L. de Boeij, M. Franchini, J. A. Groeneveld, E. S. Kadantsev, R. Klooster, F. Kootstra, M. C. W. M. Pols, P. Romaniello, M. Raupach, D. G. Skachkov, J. G. Snijders, C. J. O. Verzijl, J.A. Celis Gil, J. M. Thijssen, G. Wiesenekker, C. A. Peeples, G. Schreckenbach and T. Ziegler, SCM BAND 2024.1, *Theoretical Chemistry, Vrije Universiteit*, Amsterdam, The Netherlands, **http://www.scm.com**.